satisfies Oswald's[2] suggestion that the best performance is realized by selecting the propeller blade angle that absorbs the maximum available power (94 kW = 126 hp) at the maximum possible level flight velocity (69.54 m/s = 228.15 ft/s) at sea level ($\sigma = 1 = \phi$). The velocity variations are shown for $C = 0$ and 0.15, and it is seen that these correspond to absolute ceilings of 7423 m (23,354 ft) and 5981 m (19,623 ft), respectively. A comparison with the flight data for this type of light airplane equipped with a variable-pitch (constant rpm) propeller indicates the absolute ceiling would be approximately 5500 m (18,000 ft).

In Fig. 2 we also show the theoretical upper limit for the rate of climb ($\mathring{h}_{mp}$) based on the so-called "ideal airplane" whose available power is independent of speed so that $\mathring{h}_{mp}$ is produced at V_{mp}, the velocity for minimum required power, as follows:

$$\mathring{h}_{mp} = (\sigma P_m - D_{mp} V_{mp})/W = \frac{\sigma P_m}{W} - \frac{4}{3^{3/4}} \lambda_s^{3/4} \lambda_p^{-1/4} / \sqrt{\sigma}$$

$$V_{mp} = V_* / 3^{1/4} \qquad C_{L_{mp}} = \sqrt{3} C_{L_*} = 1.24 \tag{14}$$

(e.g., see Eq. 28 of Ref. 1). However, as first pointed out by Oswald,[2] the actual minimum power nearly always occurs at a flight velocity considerably greater than V_{mp}, but less than V_*. Therefore we also show the rate of climb ($\mathring{h}_*$) at the climbing velocity V_* with the same assumption of power available being independent of speed, so that for constant $C_{L_*} = 0.714$,

$$\mathring{h}_* = (\sigma P_m / W) - 2\lambda_s^{3/4} \lambda_p^{-1/4} / \sqrt{\sigma} \tag{15}$$

Figure 2 clearly indicates that Eq. (15) for $\mathring{h}_* = 0$ with $C = 0.15$ gives a much better approximation to the actual absolute ceiling at $\sigma_h = 0.5342$ corresponding to 6073 m (19,923 ft), than does the value from Eq. (14) for $\mathring{h}_{mp} = 0$ and $C = 0.15$, which is $\sigma_h = 0.5021$, corresponding to 6626 m (21,738 ft). Figure 2 clearly shows that the assumption of $\sigma = \phi$ ($C = 0$) results in a much too high estimate of the ceiling. The reason why Eq. (14) usually overestimates the rate of climb is that $C_{L_{mp}}$ is too large to justify the use of the constant values of λ_p and λ_s, as seen in Fig. 1 of Ref. 1. On the other hand Eq. (15) corresponds to $C_{L_*} < 1$ so its predictions are more valid, although as seen in Fig. 2, $\mathring{h}_*$ can be exceeded by the rate of climb (w) from Eq. (12) for a fixed-pitch propeller because at the higher altitudes $C_{L_w} > C_{L_*}$. However, the predictions from Eq. (12) are valid for the example used in Figs. 1 and 2, since the C_L involved are all less than $C_{L_h} = 0.888$, and therefore the use of the constant values of λ_p and λ_s are justified. It should be noted that Fig. 2 confirms Oswald's[2] opinion that the best performance of a fixed-pitch propeller occurs when the propeller blade angle is selected to absorb the engine's sea level maximum P_m at the maximum possible steady level flight velocity. Oswald's propeller selection performs excellently as the altitude increases, nearly matching the ideal airplane with constant power assumption while still maintaining the basis of Eq. (1) with constant values for λ_p and λ_s, since $C_{L_w} \leq 0.888$.

The important restriction on Eqs. (12) and (13) is that C_{L_w} must not greatly exceed unity in order to justify the application of Eqs. (1) and (2). For example, if the propeller blade angle is decreased so that $V_m = (\lambda_p \lambda_s)^{1/4} = 38.2$ m/s (125.3 ft/s) in order to increase the rate of climb at sea level by 54%, then as the altitude increases, Eq. (12) predicts such low values for V_w that $C_{L_w} > 1$ for $\phi < 0.8$, the maximum value of $C_{L_w} = 1.48$ occurs at $\phi_h = 0.42$, and because the drag predicted by Eq. (1) is exceeded, Eq. (13) overestimates the rate of climb. In this case it is better to assume that the climb occurs at the constant values of $C_{L_*} = 0.7141$ and $D_* = 747.5$ N (168 lb) at the climbing velocity given by $V_* = (\lambda_p \lambda_s)^{1/4} / \sqrt{\sigma}$, so the rate of climb is given by

$$w_* = \left(\frac{T_* - D_*}{W}\right) V_* = \left[\tau_* \left(\phi - \frac{1}{3}\right) - \frac{D_*}{W}\right] \frac{(\lambda_p \lambda_s)^{1/4}}{\sqrt{\sigma}} \tag{16}$$

where

$$\tau_* = \frac{3}{2} \frac{P_m / W}{(\lambda_p \lambda_s)^{1/4}} \qquad \nu_*^{-1} = \frac{\tau_*}{3(\lambda_p \lambda_s)^{1/2}}$$

Figure 2 indicates that Eqs. (15) and (16) may provide a satisfactory upper and lower limit for the rate of climb for any variable pitch propeller. Equation (16) yields $\sigma_h = 0.5359$, giving an absolute ceiling of 6044 m (19,829 ft) for $C = 0$, and 4929 m (16,174 ft) for $C = 0.15$. The latter is too low, so a calculation with $C = 0.0732$ gives an absolute ceiling of 5500 m (18,000 ft), which is reasonable. This shows how important the determination of $\phi(\sigma)$ is for performance prediction as the altitude increases. Perhaps a review of existing flight data could produce a better relation for ϕ/σ than the empirical relation used in Eq. (3) and in Refs. 1 and 2.

Finally, Fig. 1 shows the velocity for the minimum value of (D/V), as given by $V/(\lambda_p \lambda_s)^{1/4} = 3^{1/4} \sigma^{-1/2}$ for $\sigma = \phi (C = 0)$. It is seen that at this "optimum cruise speed,"[3] the Oswald fixed-pitch propeller Eq. (7), is as effective as Eq. (11), the upper limit for a variable-pitch propeller whose power output does not decrease with speed.

References

[1] Laitone, E.V., "Performance Prediction for Light Airplanes," *Journal of Aircraft*, Vol. 18, Nov. 1981, pp. 968-991.

[2] Oswald, B.W., "General Formulas and Charts for the Calculation of Airplane Performance," NACA TR 408, 1932.

[3] Carson, B.H., "Fuel Efficiency of Small Aircraft," *Journal of Aircraft*, Vol. 19, June 1982, pp. 473-479.

Transonic Shock/Turbulent Boundary-Layer Interaction on Curved Surfaces

George R. Inger*
University of Colorado, Boulder, Colorado

Introduction

An understanding of transonic shock/boundary-layer interaction (SBLI) is important in the aerodynamic design of high-speed aircraft wings (both ordinary and circulation controlled), turbine and cascade blades in turbomachinery, and air-breathing engine inlets and diffusors. Since these applications often involve curved surfaces, and since a singularity is associated with a normal shock on a curved surface in purely inviscid flow,[1] the influence of wall curvature on transonic shock/boundary-layer interaction is an important basic and practical question. This problem is addressed here for the case of nonseparating high Reynolds number ($10^5 < Re_L \leq 10^8$) turbulent boundary layers on convex surfaces with a curvature boundary-layer thickness product $K\delta_0$ in the practical range of $0 \leq K\delta_0 \leq 0.02$.

Presented as Paper 81-1244 at the AIAA 14th Fluid and Plasma Dynamics Meeting, Palo Alto, Calif., June 23-25, 1981; submitted Nov. 15, 1982; revision received Nov. 18, 1982.

*Professor and Chairman, Aerospace Engineering Sciences Department.

Theoretical Model

It is an experimental fact[2] that the transonic SBLI interaction pattern for the present problem is of the simpler type illustrated in Fig. 1a. The boundary layer spreads out the shock pressure perturbation (Fig. 1b) with a corresponding increase in displacement thickness behind the shock (Fig. 1c) that can significantly affect the overlying inviscid flow even with an otherwise very thin undisturbed boundary layer. A realistic model of the true outer inviscid flow in the interaction zone must at the very least account for this change in the effective body slope and position at the shock foot.

At high Reynolds numbers the interactive perturbation field organizes into a basic triple-deck structure (Fig. 1a) consisting of an outer potential inviscid flow region containing the incident shock and interactive wave systems, a middle deck of frozen shear stress/rotational inviscid disturbance flow occupying most of the incoming boundary-layer thickness, and an inner shear disturbance wall sublayer containing the interactive skin friction perturbations (and hence any possible incipient separation) plus most of the upstream influence. This disturbance field has been analyzed by extending to curved walls a fully turbulent version[3] of Lighthill's[4] nonasymptotic triple-deck interaction theory, which has been extensively validated by experiment.[5] The incoming turbulent boundary-layer profile is treated by an analytical law of the wall/wake model[6] that involves four arbitrary parameters: preshock Mach number, displacement thickness Reynolds number, incompressible shape factor H_{i_1}, and $K\delta_0$. Wall curvature can alter the interactive behavior by influencing the outer inviscid flow, shock wave location and shape and the incoming undisturbed boundary-layer velocity profile and eddy viscosity, while introducing new perturbation terms of order $K\delta_0$ into the disturbance equations for the various decks.

The curvature effect on the unperturbed outer-deck inviscid flowfield and its attendant shock location are automatically accounted for by whatever global inviscid solution code is being used for the given curved body (note that the present interaction theory describes perturbations *relative* to this inviscid shock location[3]); the resulting "bare body" inviscid solution possesses a well-known logarithmic pressure singularity at the surface due to its curvature.[1] A detailed hodograph analysis of the transonic perturbation flow[7] shows that while the explicit new curvature terms in the disturbance flow equations are of the negligible order $K\delta_0$, the interactive viscous displacement effect from the underlying decks eliminates the aforementioned inviscid singularity while slightly altering the shock into a somewhat oblique configuration. To see this, note that the local inviscid perturbation field pertains to an effective body consisting of the bare wall $h_w = h_1 = C_1X^2$ *plus* a slope jump C_2 at the shock foot followed by further growth due to the interactive displacement thickness effect, giving $h_2 = h_{w_{\text{eff}}} = C_2X + D_2X^2$ (Fig. 2b). Analysis[7] of the local disturbance flow upstream and downstream of the shock foot then yields *two* solution possibilities, one regular and the other singular, depending upon whether the interactive deflection effect is included ($C_2 > 0$, $D_2 \neq C_1$) or neglected a priori ($C_2 = 0$, $D_2 = C_1$); as shown in Fig. 2, the latter case pertains to the singular inviscid solution for a normal shock on a curved surface (Fig. 2a), while the former is the physically correct interactive solution with a slightly oblique shock. This important result is corroborated by numerical transonic inviscid flowfield studies on supercritical airfoils[8] (see Fig. 3): inclusion of the interactive influence by means of a viscous displacement "bump" eliminates the shock foot singularity that otherwise occurs.

Detailed examination of the middle-deck region again shows that any new terms in the inviscid rotational disturbance equations are of the negligible order $K\delta_0$: only the curvature effect on the *undisturbed* boundary-layer velocity and eddy viscosity profiles are of possible significance. Here

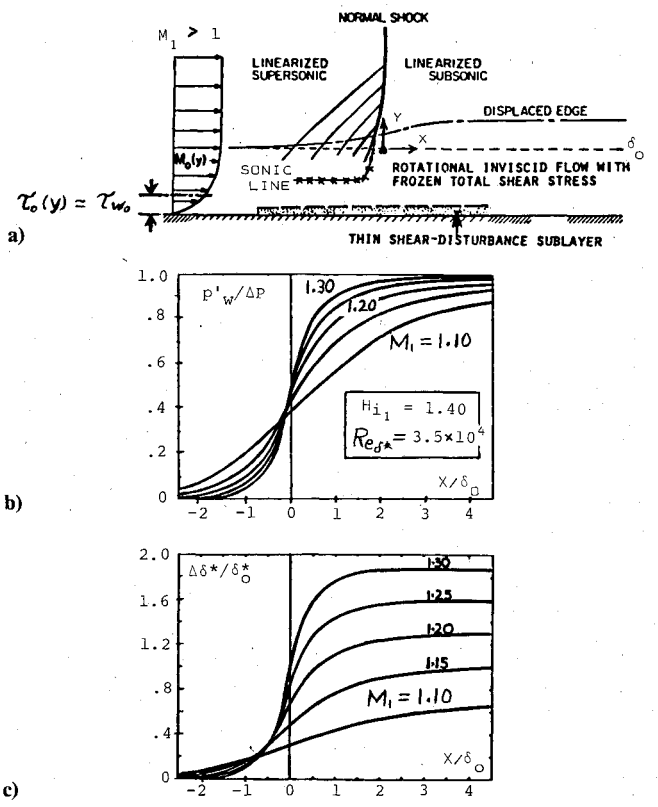

Fig. 1 Typical triple-deck structure and properties of a nonseparating turbulent transonic SBLI region. a) Flow structure. b) Wall pressure. c) Displacement thickness.

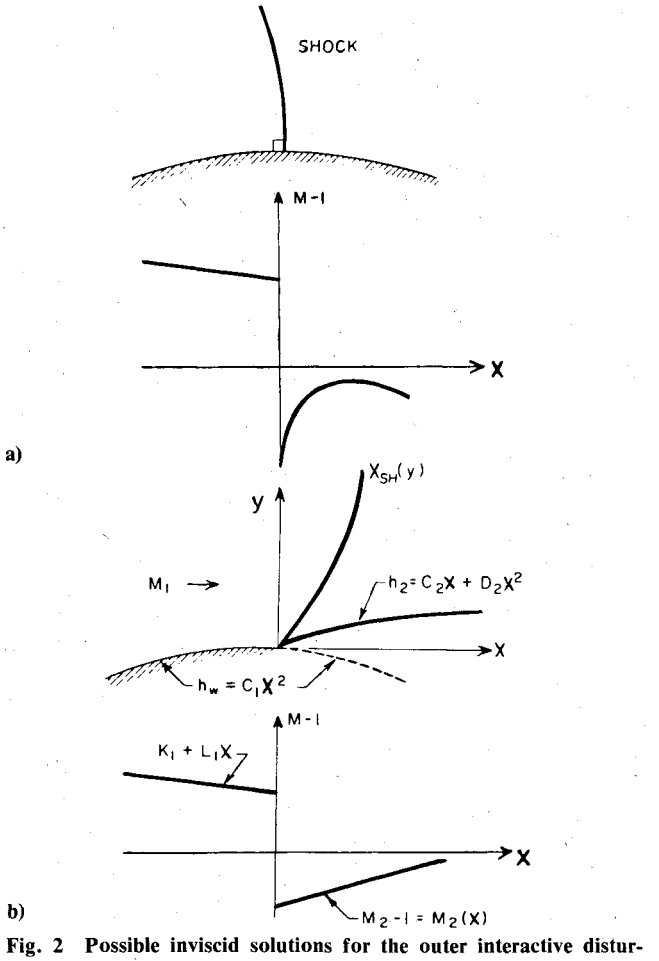

Fig. 2 Possible inviscid solutions for the outer interactive disturbance flow on a curved wall. a) Singular: viscous displacement effect neglected. b) Regular: viscous displacement effect included.

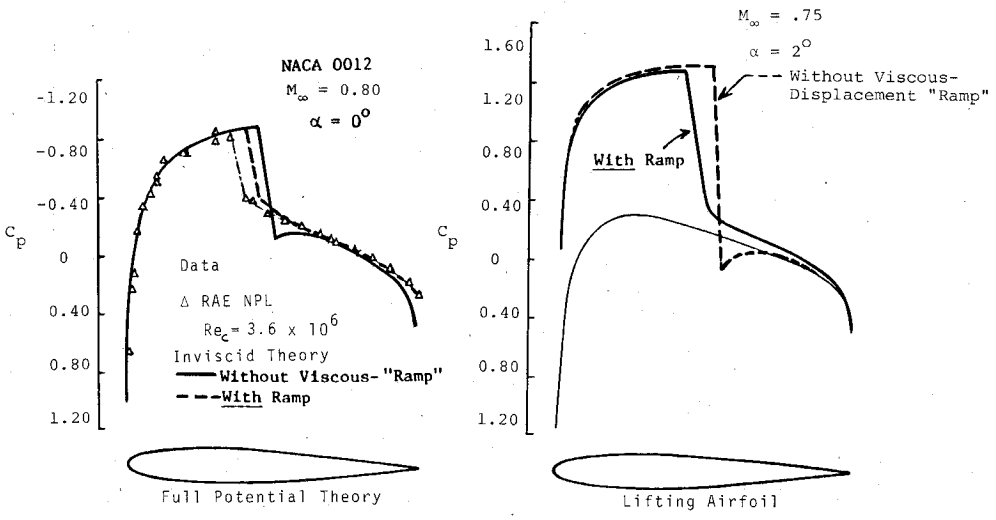

Fig. 3 Elimination of the shock-curved wall singularity by the interactive viscous displacement effect: supercritical airfoil flow-field calculations.

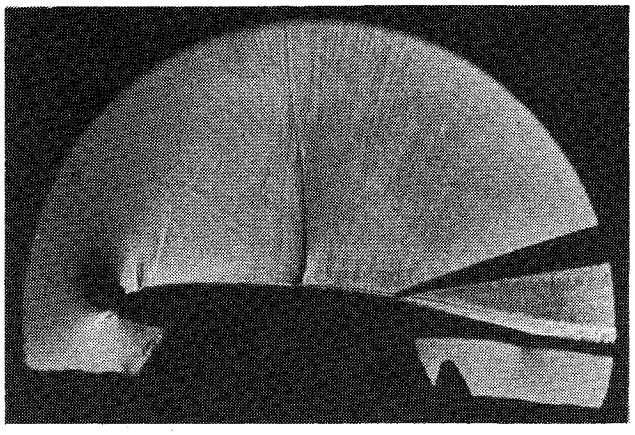

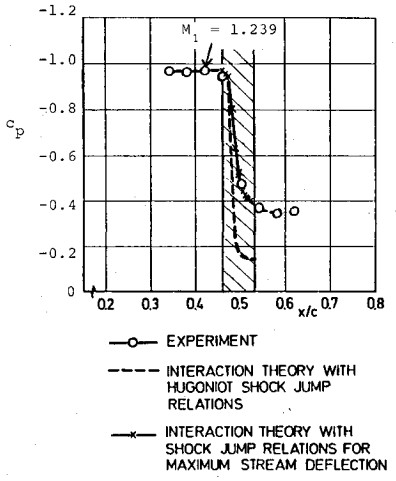

Fig. 4 Shock obliquity due to viscous interaction.

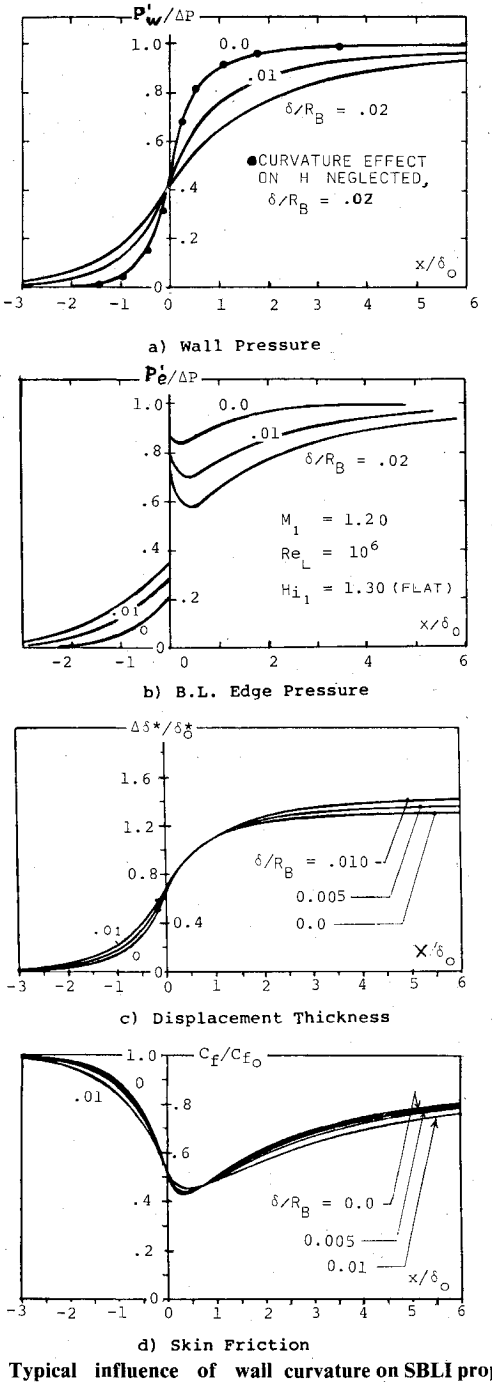

Fig. 5 Typical influence of wall curvature on SBLI properties.

again, the explicit $K\delta_0$ terms in the governing equations of this incoming flow are all negligible; however, curvature can moderately influence (10-20%) the eddy viscosity terms,[9] with a consequent effect on the boundary-layer profile in the form of a skin friction reduction and shape factor increase as described approximately by the relationships

$$C_{f_0} \approx (1 - 10K\delta_0)\,[C_{f_0}]_{\text{flat}} \tag{1}$$

$$H_{i_1} \approx (1 + 5K\delta_0)\,[H_{i_1}]_{\text{flat}} \tag{2}$$

where to this order of accuracy the corresponding effect on δ_0 is negligibly small. Note, for example, that the typical value $K\delta_0 \approx 0.01$ yields a reduction and increase in C_{f_0} and H_{i_1} of

10 and 5%, respectively. The use of Eqs. (1) and (2) with the Walz velocity profile model and $K\delta_0$ as an additional input parameter provides a good engineering account of the moderate curvature effects on the middle-deck interaction solution. The attendant slight shock obliquity effect due to the regular interactive flow and the outer edge mentioned above is accounted for by utilizing the experimental observation[10] (see, e.g., Fig. 4) that the resulting postshock flow is essentially sonic and hence has a pressure rise equivalent to a normal shock at the effective lower Mach number

$$M_{1_{\text{eff}}} \simeq M_1 \sin(90^\circ - 37.3\sqrt{M_1 - 1}) \qquad (3)$$

Within the very thin inner disturbance shear stress deck it is found yet again that the explicit curvature effects on the various inertia, pressure gradient, and laminar viscous terms in the disturbance flow equations are altogether negligible (indeed, even more so than for the middle deck since now they are of order $K\delta_{\text{ID}}$ where the inner-deck thickness $\delta_{\text{ID}} \ll \delta_0$). What remains, then, is the possible effect on both the undisturbed and perturbation turbulent eddy viscosity (note that the latter is automatically negligible in the overlying middle deck by virtue of the frozen turbulence approximation therein). This question was carefully studied[11] using the Cebeci eddy viscosity model including longitudinal curvature.[12] It was found that because of the extreme inner-deck thinness, the eddy viscosity curvature effect therein can be safely neglected for the high Reynolds number conditions typifying most practical external aerodynamic flows. Also, this curvature has a noticeable effect only at the lower Reynolds number conditions $Re_L < 10^5$ pertaining to turbomachinery blade flows.

Discussion of Results

The foregoing theoretical model accounts for the essential effects of wall curvature while containing sufficient parametric flexibility to assess the magnitude of these effects over a wide range of conditions. Results showing the typical influence of the curvature parameter $K\delta_0$ on a SBLI zone are presented in Fig. 5. It is seen that curvature slightly spreads out the interaction, weakening the adverse pressure gradient along the wall (Fig. 5a), due primarily to the increased shape factor. The attendant boundary-layer edge pressure (Fig. 5b) shows that a small *subsonic* expansion region occurs right behind the shock regardless of wall curvature; this is an inherent regular local feature of the viscous-inviscid interaction even on a flat surface.[11,13] Since the curvature slightly reduces the incoming boundary-layer velocity profile fullness and spreads out the interaction, it further acts to thicken the downstream boundary layer (Fig. 5c). Moreover, although curvature reduces the upstream skin friction, Fig. 5d shows that it slightly *increases* the local C_f around the shock foot owing to the reduced interactive pressure gradient. This is concordant with Gadd's assertion[14] that convex surface curvature slightly delays incipient separation (see Ref. 13 for more details).

Acknowledgment

This research was supported by the Office of Naval Research under Contract NR-061-274, Dr. Robert Whitehead technical monitor.

References

[1]Oswatitsch, K. and Zierep, J., "Das Problem des Senkrechten Stosses an einer Gekrümmten Wand," *ZAMM*, Vol. 40, 1960, p. 143.

[2]Ackeret, J., Feldman, F., and Rott, N., "Investigation of Compression Shocks and Boundary Layers in Gases Moving at High Speed," NACA TN-1113, 1947.

[3]Inger, G.R., "Upstream Influence and Skin Friction in Non-Separating Shock-Turbulent Boundary Layer Interactions," AIAA Paper 80-1411, 1980.

[4]Lighthill, M.J., "On Boundary Layers and Upstream Influence, II. Supersonic Flow Without Separation," *Proceedings of the Royal Society of London*, Vol. A217, 1953, pp. 478-507.

[5]Inger, G.R., "Some Features of a Shock-Turbulent Boundary Layer Interaction Theory in Transonic Flow Field," *Proceedings of AGARD Symposium on Computation of Viscous-Inviscid Interactions*, 1980, pp. 18-1-18-66.

[6]Walz, A., *Boundary Layers of Flow and Temperature*, MIT Press, Cambridge, Mass., 1969, p. 113.

[7]Sobieczky, H., "A Computer Program for Analysis of Transonic Flows Past a Wall Ramp," Engineering Experiment Station, College of Engineering, University of Arizona, Tucson, June 1978.

[8]Jau, W.H. and Murman, E., "A Phenomenological Model for Displacement Thickness Effects of Transonic Shock Wave-Boundary Layer Interactions," *AGARD Conference on Viscous-Inviscid Interactions*, Paper 15, 1980.

[9]Bradshaw, P., "Effects of Streamline Curvature on Turbulent Flow," AGARDograph 169, 1973.

[10]Nandanan, M., Stanewsky, E., and Inger, G.R., "A Computational Procedure for Transonic Airfoil Flow Including a Special Solution for Shock-Boundary Layer Interaction," AIAA Paper 80-1389, 1980.

[11]Inger, G.R. and Deane, A., "Transonic Shock-Turbulent Boundary Layer Interaction in Curved Boundary Layers with Tangential Injection," ONR report, in preparation.

[12]Cebeci, T., "Wall Curvature and Transition Effects in Turbulent Boundary Layers," *AIAA Journal*, Vol. 9, Sept. 1971, pp. 1868-1870.

[13]Inger, G.R., "Transonic Shock-Turbulent Boundary Layer Interaction and Incipient Separation on Curved Surfaces," AIAA Paper 81-1244, 1981.

[14]Gadd, G.E., "Interactions Between Normal Shock Waves and Turbulent Boundary Layers," British ARC 22559, R&M 3262, 1962.

Disadvantages of Thin Airfoil Formulations for Closely Coupled Airfoils

Kamran Rokhsaz* and Bruce P. Selberg†
University of Missouri-Rolla, Rolla, Missouri

Nomenclature

AOA	= angle of attack of the lower airfoil
C_l	= lift coefficient
C_{l_0}	= lift coefficient at zero angle of attack
$\bar{C}_l$	= average lift coefficient
ΔC_m	= additional pitching moment
D	= decalage, positive for upper wing at higher incidence
G	= nondimensional vertical distance with respect to airfoil chord
S	= nondimensional horizontal distance, positive for upper wing leading the lower wing

Introduction

FOR incompressible inviscid flow the lift and moment coefficients can be predicted by superposition of the effects of angle of attack (AOA) and the effect of the curvature of the mean camber line. This is because both the governing differential equations and the boundary conditions are linear. This technique has been widely used successfully

Received Nov. 12, 1982; revision received Dec. 17, 1982.

*Graduate Student, Mechanical and Aerospace Engineering. Student Member AIAA.

†Professor of Aerospace Engineering, Mechanical and Aerospace Engineering. Member AIAA.